2013 International Nuclear Atlantic Conference - INAC 2013
Recife, PE, Brazil, November 24-29, 2013
ASSOCIAÇÃO BRASILEIRA DE ENERGIA NUCLEAR - ABEN
***ISBN*: 978-85-99141-05-2**

COMPUTATIONAL SIMULATION OF TURBULENT NATURAL CONVECTION IN A CORIUM POOL

Camila B. Vieira[1], Bojan Ničeno[2] and Jian Su[1]

[1]Programa de Engenharia Nuclear, COPPE
Universidade Federal do Rio de Janeiro
Avenida Brigadeiro Trompowski, s/n - Cidade Universitária
21941-972 Rio de Janeiro, RJ
camila@lasme.coppe.ufrj.br
sujian@lasme.coppe.ufrj.br

[2]Nuclear Energy and Safety
Paul Scherrer Institut,
5232 Villigen PSI
Switzerland
bojan.niceno@psi.ch

ABSTRACT

After a severe accident in a nuclear power plant, the total thermal loading on the vessel of a nuclear reactor is controlled by the convective heat transfer. Taking that fact into account, this work aimed to analyze the turbulent natural convection inside a representative lower head cavity. By means of an open-source CFD code, OpenFOAM (Open Field Operation and Manipulation), numerical simulations were performed to investigate a volumetrically heated fluid ($Pr = 7.0$) at internal Rayleigh (Ra) numbers ranging from 10^8 to 10^{15}. Bearing in mind that severe accident scenario and the physical-chemical effects are many and complex, the fluid analyzed was considered Newtonian, with constant physical properties, homogeneous and single phase. Even working with that simplifications, the modeling of turbulent natural convection has posed a considerable challenge for the Reynolds Averaged Navier-Stokes (RANS) equations based models, not only because of the complete unsteadiness of the flow and the strong turbulence effects in the near wall regions, but also because of the correct treatment of the turbulent heat fluxes ($\overline{\theta u_i}$). So, this work outlined three approaches for treating the turbulent heat fluxes: the Simple Gradient Diffusion Hypothesis (SGDH), the Generalized Gradient Diffusion Hypothesis (GGDH) and the Algebraic Flux Model (AFM). Simulations performed at BALI test based geometry with a four equations model, k-ε-$\overline{v^2}$-f (commonly called as $\overline{v^2}$-f and V2-f), showed that despite of AFM and GGDH have provided reasonable agreement with experimental data for turbulent natural convection in a differentially heated cavity, they proved to be very unstable for buoyancy-driven flows with internal source in comparison to SGDH model.

1. INTRODUCTION

Severe accident in nuclear power plants is a relatively rare occurrence, but due to its potential impact on the environment, it is vigorously studied in the last few decades. It is caused by a long absence of the core cooling. Under such condition, the core is overheated and a melt pool might form in the lower plenum of the reactor vessel.

After the initial melting of the core, the molten mixture constituted by portions of reactor core, so called corium, can be stratified with a metallic layer, composed mainly by the reflector, steel, iron and zircaloy, above an oxidic pool constituted mostly by ZrO_2 and

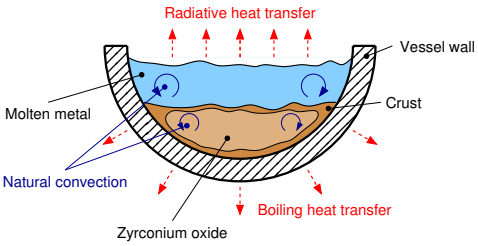

Figure 1: Corium configuration with a metallic layer bellow the oxide material.

UO_2. Some oxide species can be reduced and transfered to the metallic layer increasing its density and consequently leading to the relocation of a metallic layer bellow the oxide pool, as it is depicted by Fig. 1.

The knowledge of the heat transfer phenomena in a molten core is essential for the lower vessel integrity. Since the total thermo-mechanical loading is basically controlled by the natural convection generated by the decay heat of the fission products, this phenomenon has been widely investigated.

In a general way, natural convection involving internal heat source can be adequately studied by two dimensionless parameters: Prandtl number, Pr, and the internal Rayleigh number, Ra_i.

$$Pr = \frac{\nu}{\alpha} \quad \text{and} \quad Ra_i = \frac{q_v g \beta H^5}{\alpha \nu \lambda},$$

in which ν is the kinematic viscosity, α the thermal diffusivity, q_v the volumetric heat source, g the gravity, β the thermal expansion coefficient, $-1/\rho(\partial\rho/\partial T)_P$, H the characteristic dimension and λ the thermal conductivity.

In order to analyze the dimensionless heat transfer, defined by the Nusselt number ($Nu = hH/\lambda$, where h is the heat transfer coefficient) in terms on the Ra number, many works aim to get correlations with Nu as function of Ra_i, as it can be found in Rempe et al. [17] paper,

$$Nu = a\, Ra_i^n.$$

The range of phenomena taking place inside the corium is immense. The Ra_i numbers of a system under severe accidents can reach order of 10^{17}, the working fluid is a non-homogeneous mixture with chemical reactions leading to hydrogen generation and intense internal heat generation, interaction with the walls of the reactor vessel, crust formation, phase separation, wall degradation, among many other phenomena that could be cited.

Scientific comprehension of all phenomena in a corium, is still not available. So, research plays an important role in accident management assessment, which has been quite studied in last years, following the Three Mile Island accident in 1979 and recently the Fukushima Daiichi nuclear accident in 2011.

Several organizations over the world conducted experiments not only to enhance the analysis of retaining the core melt inside the Reactor Pressure Vessel (RPV) but also to understand the fundamental behavior of the molten pool inside the RPV, for both homogeneous and stratified configuration of the molten pool. Some experiments which were performed to reach that goal are COPO I and II (Finland and France), ACOPO

(USA) (Theofanous et al. [19]), RASPLAV (Russia) and BALI (France) (Bonnet and Seiler [1]).

Among the experiments cited above, one of the most known experiments which was designed to investigate the thermal hydraulics of a corium pool for both in-vessel and ex-vessel situation is BALI experiment. It was developed to provide a data base on heat transfer distribution at melt pool boundaries for Rayleigh numbers in the range of 10^{16} to 10^{17}. Bonnet and Seiler [1] presented BALI results of axial temperature and heat flux distributions along the pool boundaries, which were the first ones obtained for a very high Ra number (10^{17}).

Clearly, due to the complexity of phenomena occurring inside the corium, numerical simulations of natural convection in molten core pools pose a noteworthy challenge for modeling, due to the inherently unsteadiness of the flow, the difficulty to model the near wall regions, the constant transition of the boundary layer regions as consequence of the unsteady flow configuration and finally the requirement of a properly modeling of the turbulent kinetic energy production due to the buoyancy.

Nevertheless, Computational Fluid Dynamics (CFD) with RANS turbulence models, or by resolving large scales of motion in the framework of Large Eddy Simulation (LES) have proved able to provide, for instance, an estimate of flow details and local heat transfer for complex flows.

Nourgaliev et al.[16] presented an analysis of Pr number effects on natural convection in different geometries (square, semicircular and hemispherical cavities) by means of simulations with standard low-Reynolds k-ε turbulence model. It was found that the Pr number had few effects on the averaged Nu numbers in the convection-dominated region (close to the top surface), while for the conduction-dominated domains (stably stratified bottom regions), the Pr number proved to have a significant effect on the heat transfer, which increased with the Ra number rise.

Fukasawa et al. [7] examined low-Reynolds number models and the LES through BALI test analysis. The analysis of axial temperature for both top cooling and adiabatic upper surface was shown. A more stable and stratified flow was found for the adiabatic boundary on the top, which also led to a small difference between the turbulence models analyzed.

The two above works made use of the SGDH approach for the treatment of the turbulent heat fluxes ($\overline{\theta u_i}$). Despite one point-closure models have proved successful in a wide range of applications, it is known that in flows driven by thermal buoyancy the deficiencies of isotropic eddy-diffusivity models can be quite evident (Hanjalić [9]). For instance, in a common heated vertical wall leading to a convective boundary layer, the main buoyancy source of the turbulent kinetic energy is associated with the vertical heat flux ($\beta g_i \overline{\theta u_i}$), which for an isotropic heat flux, with negligible mean temperature gradient in the vertical direction, contrary to the physics of a buoyancy-driven turbulence, it is not taken into account.

The GGDH proposed by Daly and Harlow [4] and Ince and Launder [10] is the simplest

closure which takes into account the temperature gradients perpendicular to gravity.

Hanjalić [9] presented an exact transport equation for the heat flux and the temperature variance, which results in a better approximation than GGDH. It was also shown a simplified AFM, above which was first introduced by Kenjereš et al. [11] and does not require solutions of differential transport equations for each flux component but still captures important physical processes, such as the mechanical, thermal and buoyancy production phenomena.

The fact that AFM and GGDH models can vary considerably from turbulence model to other makes its application quite limited. For instance, Choi et al. [3] used AFM for the heat flux calculation in order to investigate its accuracy and stability in addition with SST and $\overline{v^2}$-f, and it was found that the performance of AFM depended strongly on the constants of the algebraic expression, for each turbulence model.

Based on the importance of the natural convection for the total thermal loading analysis in a molten core and consequently for accident management assessments, in addition to the role of CFD simulations for a better comprehension of phenomena taking place inside an oxide layer of a corium after a sever accident, this work had as objective the investigation of three different approaches (SGDH, GGDH and AFM) for the turbulent heat fluxes modeling, outlining the advantages and deficiencies of each one for buoyancy-driven flows generated by internal heat source. Making use of the same geometry and boundary conditions of BALI test facility with different aspect ratios, it will be discussed results provided by $\overline{v^2}$-f turbulence model for a fluid with $Pr = 7.0$ and Ra numbers ranging from 10^8 to 10^{15}.

2. GOVERNING EQUATIONS AND NUMERICAL METHOD

The analysis of the turbulent natural convection is mathematically described by the equations for conservation of mass, momentum and energy. This work applied the RANS methodology for solving that respective equations, for an incompressible buoyancy-driven flow with volumetrically heat generation. Assuming the Boussinesq approximation, the governing equations for this problem are,

$$\frac{\partial U_i}{\partial x_i} = 0, \tag{1}$$

$$\frac{\partial U_i}{\partial t} + U_j \frac{\partial U_i}{\partial x_j} = -\frac{\partial P}{\partial x_i} + \frac{\partial}{\partial x_j}\left[\nu\left(\frac{\partial U_i}{\partial x_j} + \frac{\partial U_j}{\partial x_i}\right) - \overline{u_i' u_j'}\right] + \beta(T - T_0)g_i, \tag{2}$$

$$\frac{\partial T}{\partial t} + U_j \frac{\partial T}{\partial x_j} = \frac{\partial}{\partial x_j}\left(\alpha \frac{\partial T}{\partial x_j} - \overline{\theta u_j'}\right) + \frac{q_v}{\rho c_p}, \tag{3}$$

in which, U_i is a component of the mean velocity, u_i' velocity fluctuation, T the mean temperature, θ temperature fluctuation, ρ the fluid density and c_p the heat capacity at constant pressure. Both the turbulent stress, $\overline{u_i' u_j'}$, and turbulent heat flux, $\overline{u_i' T'}$, represent the unresolved turbulence contributions, which need to be modeled in order to close the above equations.

The turbulent stress $\overline{u_i' u_j'}$ was given by the Boussinesq hypothesis as follows:

$$\overline{u_i' u_j'} = \frac{2}{3} k \delta_{ij} - \nu_t \frac{\partial U_i}{\partial x_j}, \tag{4}$$

where k is the turbulence kinetic energy, ν_t is the eddy viscosity.

According to the $\overline{v^2}$-f model applied in this work, which was based on the modifications proposed by Davidson and Nielsen [5], ν_t was calculated as following,

$$\nu_t = min\left[C_{\mu,k\varepsilon}\frac{k^2}{\varepsilon}, C_\mu \overline{v^2}\tau\right], \tag{5}$$

in which ε is the kinetic energy dissipation rate, $\overline{v^2}$ the magnitude of the velocity fluctuations normal to the flow direction and τ the time scale.

The implementation applied by the present work used both in time scale and length (L) scales, the limits of Kolmogorov variables, in order to avoid singularities in the governing equations in the near-wall regions. The limits here used were ensured to be activated in regions for $y^+ < 30$, as can be observed by the equations (6) and (7),

$$\tau = max\left[\frac{k}{\varepsilon}, pos(30 - y^*)6\sqrt{\frac{\nu}{\varepsilon}}\right], \tag{6}$$

$$L = C_L max\left[\frac{k^{3/2}}{\varepsilon}, pos(30 - y^*)C_\eta \left(\frac{\nu^3}{\varepsilon}\right)^{1/4}\right], \tag{7}$$

where ν is the kinematic viscosity and y^* was calculated according to the equation (8),

$$y^* = \frac{C_{\mu,k\varepsilon}^{1/4} k^{1/2} y_n}{\nu}, \tag{8}$$

in which y_n is the distance of the first near-wall cell center.

The main set of equations of $\overline{v^2}$-f applied in this work can be described by the next four equations, which are respectively the transport equations of k, ε, $\overline{v^2}$ and an elliptic equation for the relaxation function (f),

$$\frac{\partial k}{\partial t} + U_j \frac{\partial k}{\partial x_j} = P_k + G_b - \frac{k}{\tau} + \frac{\partial}{\partial x_j}\left[\left(\nu + \frac{\nu_t}{\sigma_k}\right)\frac{\partial k}{\partial x_j}\right], \tag{9}$$

$$\frac{\partial \varepsilon}{\partial t} + U_j \frac{\partial \varepsilon}{\partial x_j} = \frac{C_{\varepsilon 1}(P_k + G_b)}{\tau} - \frac{C_{\varepsilon 2}\varepsilon}{\tau} + \frac{\partial}{\partial x_j}\left[\left(\nu + \frac{\nu_t}{\sigma_\varepsilon}\right)\frac{\partial \varepsilon}{\partial x_j}\right], \tag{10}$$

$$\begin{aligned}\frac{\partial \overline{v^2}}{\partial t} + U_j \frac{\partial \overline{v^2}}{\partial x_j} = min\left[kf, -\frac{1}{\tau}\left((C_1 - 6)\overline{v^2} - \frac{2}{3}k(C_1 - 1)\right)\right] \\ -\frac{6\overline{v^2}}{\tau} + \frac{\partial}{\partial x_j}\left[\left(\nu + \frac{\nu_t}{\sigma_{\overline{v^2}}}\right)\frac{\partial \overline{v^2}}{\partial x_j}\right],\end{aligned} \tag{11}$$

$$\frac{\partial^2 f}{\partial x_j^2} = \frac{f}{L^2} - \frac{1}{L^2\tau}\left[(C_1 - 6.0)\frac{\overline{v^2}}{k} - (C_1 - 1)\frac{2}{3}\right] - \frac{C_2(P_k + G_b)}{k}, \tag{12}$$

in which the buoyancy production term, G_b, was defined as following,

$$G_b = -\beta g_j(\nu_t/Pr_t)(\partial T/\partial x_j), \tag{13}$$

where g_j is the gravity and Pr_t the turbulent Prandtl, which was considered equal to 0.9.

The coefficients used in this turbulence model were defined as,

$$C_\mu = 0.22, \quad C_{\mu,k\varepsilon} = 0.09, \quad C_{\varepsilon 2} = 1.90,$$

$$C_{\varepsilon 1} = 1.40(1 + 0.05min(k^{1/2}/\overline{v^2}, 10.0)),$$

$$C_1 = 1.40, \quad C_2 = 0.30, \quad C_L = 0.23, \quad C_\eta = 70.0,$$

$$\sigma_k = \sigma_{\overline{v^2}} = 1.0, \quad \sigma_\varepsilon = 1.3.$$

The boundary conditions at solid walls were $U_i = 0$, $T = T_0$, $\varepsilon = 2\nu k/y_n^2$ (calculated by means of first cell centre values of k from the wall), $f = 0$, $\overline{v^2} = 0$. In order to close the set of equations (1 – 3), it was investigated three different approaches for the turbulent heat fluxes $\overline{\theta u_i'}$ calculation: the SGDH, which implies the isotropic eddy-diffusivity,

$$\overline{\theta u_i'} = -\frac{\nu_t}{Pr_t}\frac{\partial T}{\partial x_i}, \tag{14}$$

the GGDH,

$$\overline{\theta u_i'} = -C_\theta \frac{k}{\varepsilon}(\zeta \overline{u_i' u_j'}\frac{\partial T}{\partial x_j}), \tag{15}$$

and the AFM, which contains the thermal (P_{th}), the mechanical (P_m) and buoyancy ($G_{\theta i}$) production terms, whose equation was based on Kenjereš [12] according to the following equation,

$$\overline{\theta u_i'} = -C_\theta \frac{k}{\varepsilon}(\zeta \underbrace{\overline{u_i' u_j'}\frac{\partial T}{\partial x_j}}_{P_{th}} + \xi \underbrace{\overline{\theta u_i'}\frac{\partial U_i}{\partial x_j}}_{P_m} + \eta \underbrace{\beta g_i \overline{\theta^2}}_{G_{\theta i}}). \tag{16}$$

The variance of temperature $\overline{\theta^2}$ is calculated by solving the following transport equation,

$$\frac{\partial \overline{\theta^2}}{\partial t} + U_j\frac{\partial \overline{\theta^2}}{\partial x_j} = -2\overline{\theta u_j'}\frac{\partial T}{\partial x_j} - 2\varepsilon_\theta + \frac{\partial}{\partial x_j}\left[\left(\nu + \frac{\nu_t}{\sigma_{\overline{\theta^2}}}\frac{\partial \overline{\theta^2}}{\partial x_j}\right)\right], \tag{17}$$

in which, $\sigma_{\overline{\theta^2}} = 1.0$ and the dissipation of the temperature variance, ε_θ, was calculated according to the following equation,

$$\varepsilon_\theta = \frac{\varepsilon \overline{\theta^2}}{2Rk}. \tag{18}$$

The thermal to mechanical time-scale ratio (R) was assumed constant and equal to 0.5, the same assumption considered by Kenjereš et al. [13] and Kenjereš [12].

The coefficients of the equations 15 and 16 presented the bellow values.

$$C_\theta = 0.15, \quad \zeta = 0.6, \quad \xi = 0.6, \quad \eta = 0.6.$$

That coefficients, also applied by Kenjereš et al. [13], were selected after some tests in a heated rectangular cavity, which will be better discussed in the Results and Discussion section.

All the simulations were performed in an open-source of CFD C++ code, OpenFOAM-1.7.1, whose numerical approach is based on collocated finite volume method, solved in segregated matrices, within an iterative sequence. For the main simulation cases, which were performed in BALI test based geometry, the discretized set of equations was solved by a solver, applied for buoyant flows. The PIMPLE algorithm was used for coupling the momentum and mass conservation equations. For spatial discretization of the gradient terms, the second order accurate central difference scheme was used as well as for the Laplacian terms. The second order accurate upwind was used for the treatment of the convection terms, whereas time integration was performed with the implicit backward Euler method.

As OpenFOAM-1.7.1 does not contain the $\overline{v^2}$-f turbulence model, it had to be inserted into its library of turbulence models. So, the equations (11)–(13) were implemented and validated with Durbin [6] data. Both the validation and the mesh sensitivity analysis were checked before its application in this work. GGDH (equation (15)) and AFM (equations (16)–(18)) had also to be inserted into the solver applied for buoyant flows, since only isotropic approximation for the turbulent heat fluxes is present in OpenFOAM. They were written inside a looping, which was executed 60 times to guarantee converged solutions (different numbers of iterations were checked and it was found that 60 was enough to make the solution to converge).

3. RESULTS AND DISCUSSION

3.1. Analysis of the SGDH, GGDH and AFM models for $\overline{\theta u_i}$ in a Rectangular Cavity

Data from Kenjereš [12] and Cheesewright and King [2] were used to evaluate the implementation of AFM, GGDH and SGDH for $\overline{v^2}$-f, in a simulation with air ($Pr = 0.71$) and $Ra = 5 \times 10^8$ in a rectangular cavity depicted in Fig. 2. The heated wall vertical cavity is a simple case which is commonly used to validate second-moment closures, since this problem involves some important phenomena, such as the near-wall turbulence effects imposed by the boundary conditions and the non viscous effects due to blockage.

It was required the use of under-relaxation factors for the turbulent heat fluxes and the variance of temperature equations. The applied values were 0.2 and 0.1, for respectively $\overline{\theta u_j}$ and $\overline{\theta^2}$ (this low value was needed in order to avoid the solution to diverge as consequence of very high $\overline{\theta^2}$ solutions). The velocity was also needed to be under-relaxed, since the gradient of velocity for this problem was high and entailed in some crashes if no

relaxation parameter was used for the momentum equation. The results shown by Figs. 3, 4 and 5 were obtained with the same solver and discretization schemes applied for BALI simulations.

Different coefficients for the GGDH equation (15), present in Table 1, were tested. The turbulence model $\overline{v^2}$-f proved to be more sensitive to the values chosen for each coefficient and just that ones from Kenjereš et al. [13] provided reasonable results, which are presented here. On the other hand, simulations with SST gave similar results for all the coefficients analyzed.

Table 1: Coefficients investigated for the GGDH equation.

Reference	C_θ	ζ
Kenjeres et al. [13]	0.15	0.6
Kenjeres [12]	0.2	1.0
Thielen et al.[20]	0.3	1.0

It can be observed from Fig. 3a that $\overline{v^2}$-f model together with both AFM and GGDH provided similar results for the vertical velocity profile, while SGDH proved to show a better behavior for the velocity, once the hydrodynamic boundary layer was almost three times thinner than the one given by AFM and GGDH models. For the $\overline{v^2}$-f simulations, the vertical turbulent heat flux component (Fig. 3c) was better predicted by AFM model, followed by GGDH and considerably underpredicted by SGDH, which provided better results for the horizontal turbulent heat fluxes (Fig. 4a). Similar results were found by Choi et al. [3], who explained that though the ($\overline{\theta u}$) was overpredicted by the anisotropic models (AFM and GGDH), that component does not have much influence on the solution, differently to the vertical turbulent heat flux component($\overline{\theta v}$), which exerts an important role in the dynamics of the turbulent kinetic energy and the overall prediction of all the other quantities.

The overview of the $\overline{v^2}$-f results is that $\overline{\theta u}$ influenced the maximum peak of velocity close to the walls, while $\overline{\theta v}$ dictated the velocity flow behavior in the mid region of the cavity.

The performance of SST with AFM, GGDH and SGDH was also checked, as it can be observed in Figs. 3b, 3d and 4b. Contrary to $\overline{v^2}$-f, both the vertical velocity and horizontal turbulent heat fluxes were similarly predicted by both anisotropic and isotropic models. Nevertheless, the vertical turbulent heat fluxes were considerably underpredicted by AFM and GGH in the near-wall region and even more by SGDH model.

Figure 5 depicts the mesh sensitivity analysis carried out with three different meshes (M1 - 80×80, M2 - 82×122 and M3 - 102×152). It could be observed that for both $\overline{v^2}$-f and SST the solutions were grid independent.

3.2. BALI simulations

Turbulent natural convection in a half of semicircular cavity containing water ($Pr = 7.0$) with internal heat source were performed to analyze the performance of the AFM, GGDH

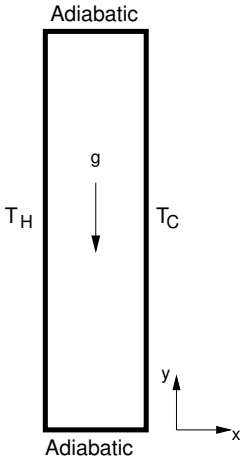

Figure 2: Scheme of the $1:5$ Heated Side Cavity, with height $H = 2.5$m and width $L = 0.5$m, used in the simulations with $Pr = 0.71$ and $Ra = 5 \times 10^8$.

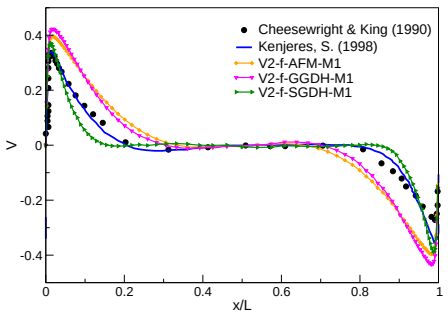

(a) V profile at $y/H = 0.5$

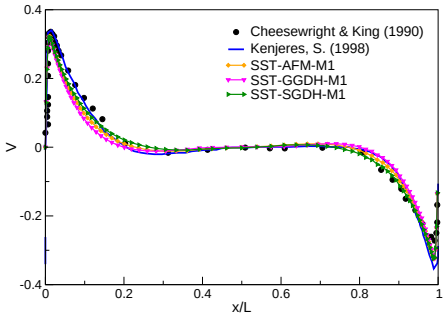

(b) V profile at $y/H = 0.5$

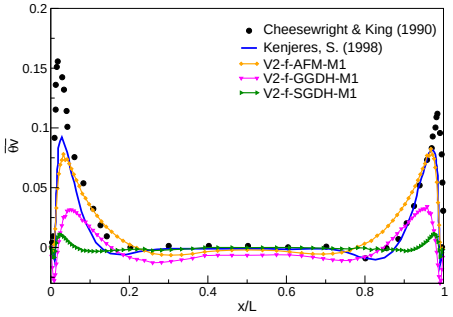

(c) $\overline{\theta v}$ profile at $y/H = 0.5$

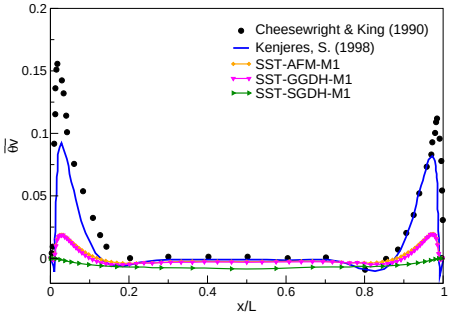

(d) $\overline{\theta v}$ profile at $y/H = 0.5$

Figure 3: Performance of (a)(c) $\overline{v^2}$-f and (b)(d) SST turbulence models with AFM, GGDH and SGDH.

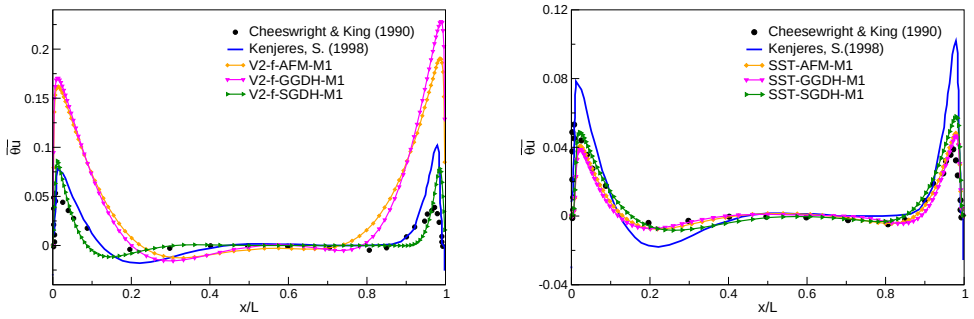

(a) $\overline{v^2}$-f (b) SST

Figure 4: $\overline{\theta u}$ profile at $y/H = 0.63$ provided by (a) $\overline{v^2}$-f and (b) SST turbulence models with AFM, GGDH and SGDH

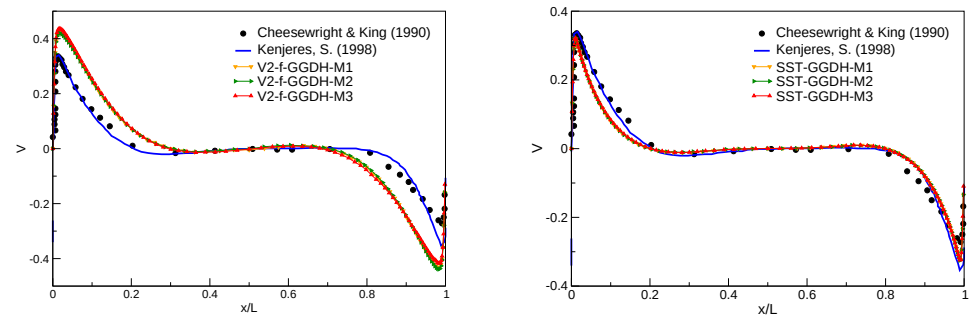

(a) $\overline{v^2}$-f (b) SST

Figure 5: Mesh Sensitivity analysis: vertical velocity profile at $y/H = 0.5$

and SGDH models for the turbulent heat fluxes calculation. The Rayleigh numbers ranged from 10^8 to 10^{15}, for simulations carried out in a geometry with aspect ratio (H/R) equal to 1 (called BALI-1), and 10^8 to 10^{12}, for a geometry with $H/R = 0.5$ (defined as BALI-2).

Figure 6 shows the boundary conditions used for both geometries here analyzed, which was an isothermal ($T_0 = 273K$) top and bottom walls (representing the oxidic crust formed around the corium, which in the experiments was reproduced by means of an ice crust) and an adiabatic side wall. The mesh used, which was clustered in the near-wall region, allowed y^+ bellow 1 in all cases here presented. At the Ra numbers ranging from 10^8 to 10^{12}, the mesh contained 298602 nodes and 148603 cells, but for $Ra \geq 10^{13}$, the mesh had to be refined to 298602 nodes and 148603 cells.

From $Ra = 10^8$ to 10^{10} the simulations converged for laminar flows and above $Ra = 10^{11}$ the turbulence model was required. Both $\overline{v^2}$-f and SST was used to check the performance of AFM, GGDH and SGDH models. The turbulence model $\overline{v^2}$-f proved to be more robust than SST at higher Ra numbers, since for Ra higher than $Ra = 10^{12}$ the SST solution diverged for all the models applied for the turbulent heat fluxes calculation. However, for $Ra = 10^{11}$, both $\overline{v^2}$-f and SST provided similar results of time and space average Nusselt number on the bottom wall ($\overline{Nu}_{dn}$), with SGDH model: 20.04 and 17.44, respectively.

Some tests with AFM were made with both $\overline{v^2}$-f and SST, but no converged solution

was found. It was tested different coefficients of the turbulent heat flux equation, initial condition, under-relaxation factors, time-steps and meshes, but no attempt resulted in a converged solution. For all the tests made, the solution diverged in few time-steps. On the other hand GGDH proved to be more stable and the simulations reached the energy conservation without crashes for Ra up to 10^{12}.

The results of $\overline{v^2}$-f with both SGDH and GGDH for $Ra = 10^{11}$ and $Ra = 10^{12}$ can be found in Table 2, which shows that GGDH model predicted higher values for $\overline{Nu}_{dn}$ in comparison to SGDH results. According to Fig. 7, in the middle of the bottom surface, GGDH provided a very high value for $\overline{Nu}_{dn}$, in the same region where it was found higher turbulence kinetic energy and velocity fields.

Table 2: Comparison of SGDH and GGDH results of $\overline{Nu}_{dn}$ with $\overline{v^2}$-f turbulence model, for BALI-2 simulations.

	$Ra = 10^{11}$		$Ra = 10^{12}$	
	SGDH	GGDH	SGDH	GGDH
$\overline{Nu}_{dn}$	20.0403	30.87	42.3839	54.8389

The local distribution of the Nusselt number along the curvilinear abscissa was analyzed for BALI-2 simulations with SGDH model for the turbulent heat fluxes. Figure 8 depicts the behavior of the heat transfer along the curvilinear abscissa (in a downward direction) and the development of the thermal boundary layer thickness (δ_{th}), which was estimated by means of the height of the cavity (H) and the time and space average $\overline{Nu}_{dn}$ number on the bottom ($\delta_{th} = H/\overline{Nu}_{dn}$).

It can be observed that close to the top the thermal boundary layer is very thin entailing in a high heat transfer and consequently higher $\overline{Nu}_{dn}$ numbers. As the end of the bottom is reached, the thermal boundary layer becomes thicker and the heat transfer decreases in consequence. Other observation is that with the increase of the Ra number the thickness of the thermal boundary layer close to the top decreases and consequently the $\overline{Nu}_{dn}$ number in that same region enhances. On the other hand, in the region close to the bottom, it cannot be predicted any tendency about the development of the thermal boundary layer as function of Ra number.

Figure 9 shows how the aspect ratio of the cavity influences the development of the

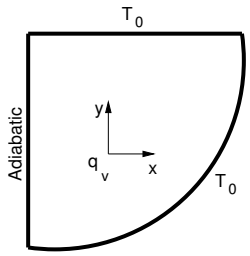

Figure 6: Scheme of the physical problem studied in BALI-1 and BALI-2 simulations.

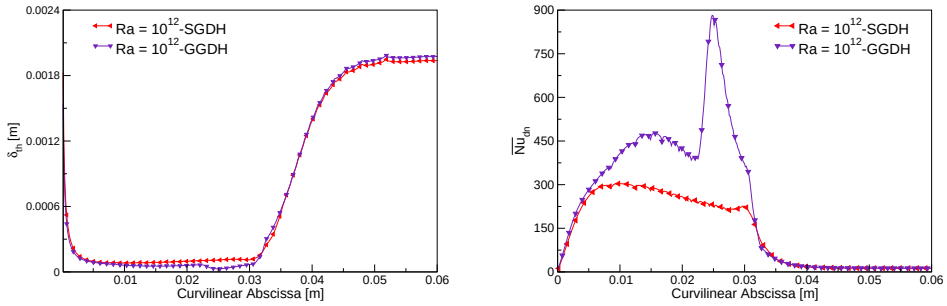

(a) (c)

Figure 7: (a) Thermal boundary layer thickness and (b) local distribution of $\overline{Nu}_{dn}$ along the bottom surface for BALI-2 simulations with both $\overline{v^2}$-f-SGDH and $\overline{v^2}$-f-GGDH models, at $Ra = 10^{12}$.

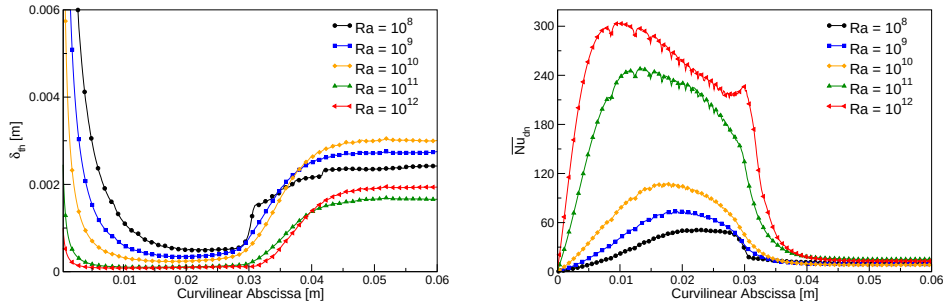

(a) (b)

Figure 8: (a) Thermal boundary layer thickness, (b) average Nusselt number along the bottom surface, for BALI-2 simulations and $Ra = 10^8 - 10^{12}$.

thermal boundary layer. It can be noted that the development of the thermal boundary layer for BALI-2, whose height is half of the radius, is smoother than it is for BALI-1. This different behavior of δ_{th} development can also contribute for the lower heat transfer rates on the bottom for BALI-2 in comparison with BALI-1, as it can be observed in Table 3.

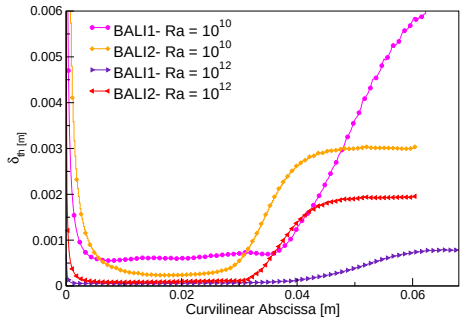

Figure 9: Thermal boundary layer thickness provided by BALI-1 and BALI-2 simulations

It can be observed by Fig.10 that $\overline{v^2}$-f-SGDH results for both BALI-1 and BALI-2 simulations were reasonable with some empirical (dashed lines) and numerical (straight line) correlations present in the literature.

Table 3: Analysis of the aspect ratio: $\overline{Nu}_{dn}$ results provided by BALI-1 and BALI-2 simulations with $\overline{v^2}$-f turbulence model at Ra numbers ranging from 10^{10} to 10^{12}.

Ra	BALI-1 ($H/R = 1$)	BALI-2 ($H/R = 0.5$)
10^{10}	16.535508	13.78563
10^{11}	28.8406	27.14984
10^{12}	47.92628	44.427578

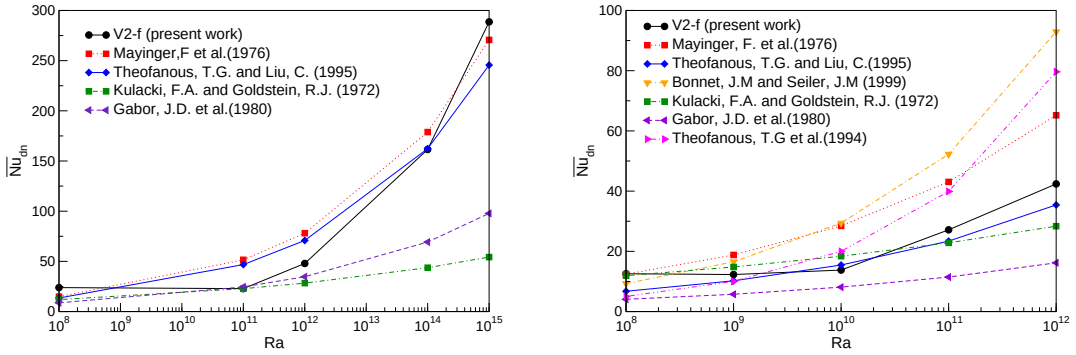

(a) (c)

Figure 10: (a) Thermal boundary layer thickness and (b) Average Nusselt number along the bottom surface.

By means of Fig. 11, it can be observed how a natural convection flows with volumetric heat source behave. According to the thermal field, one can see a stratified lower portion (conduction-dominated region) and a well-mixed upper pool region (convection-dominated region). From the flow field, it can be noticed a thin hydrodynamic boundary layer that descends downwards along the curved wall.

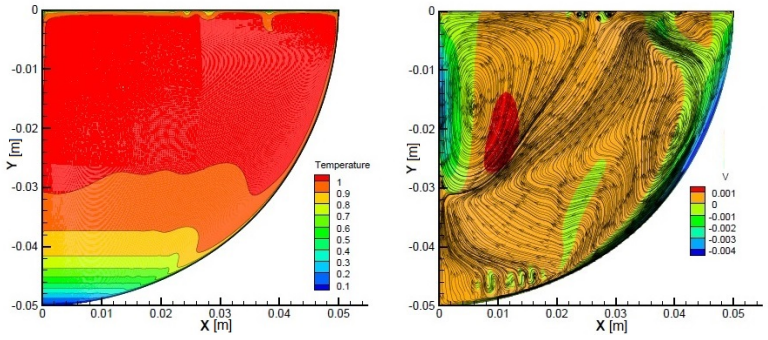

(a) (b)

Figure 11: (a) Nondimensional temperature field and (b) velocity fields computed with $\overline{v^2}$-f-SGDH for $Pr = 7.0$ and $Ra = 10^{14}$ in BALI-1 geometry.

4. CONCLUSIONS

Natural convection in cavities containing fluids volumetrically heated was investigated by means of CFD simulations, making use of $\overline{v^2}$-f and SST turbulence models in addition to three different approaches (SGDH, GGDH and AFM) for the turbulent heat fluxes treatment. In a calibration test carried out in a heated vertical cavity to check the implementation of the GGDH and AFM equations, it was observed the sensibility of each turbulence model analyzed and their performances with each turbulent heat fluxes approximation.

By means of simulations carried out in cavities with the same geometry and boundary conditions of BALI experiment, it was found that $\overline{v^2}$-f was more robust than SST, for Ra numbers above 10^{12}, but both turbulence models provided similar results for a $Ra = 10^{11}$ case. The anisotropic models GGDH and AFM had a reasonable application to the calibration test in a heated wall cavity, but the same was not observed for the natural convection with internal heat source.

Despite the simple gradient diffusion hypothesis SGDH does not take into account the flux anisotropy parameters and have provided the worst results for the turbulent heat fluxes in simulations of natural convection generated by differentially heated walls, for the cases with volumetric heat source it proved to be suitable and more stable than the anisotropic models.

ACKNOWLEDGMENTS

The authors gratefully acknowledge the financial support provided by Conselho Nacional de Desenvolvimento Científico e Tecnológico (Brazil) and Paul Scherrer Institut (Switzerland) during the realization of this work.

REFERENCES

1. Bonnet, J.M. and Seiler, J.M. Thermal hydraulic phenomena in corium Pools: the BALI experiment. *In:* 7^{th} *International Conference on Nuclear Engineering (ICONE)*, Tokyo, Japan, (1999).
2. Cheesewright, R. and King, K.J. Stress distributions in turbulent natural convection in a rectangular air cavity, *In Proceedings* 9^{th} *International Heat Transfer Conference*, Jerusalem, Israel, (1990).
3. Choi, S. and Kim, E. and Wi, M. and and Kim, S. Computation of a Turbulent Natural Convection in a Rectangular Cavity with the Low-Reynolds-Number Differential Stress and Flux Model, *KSME International Journal*, *18*, pp. 1782–1798, (2004).
4. Daly, B.J. and Harlow, F.H. Transport equations in turbulence, *Physics of Fluid*, *13*, pp. 2634–2649, (1970).
5. Davidson, L. and Nielsen, P.V. and Veningsson, A. Modifications of the $\overline{v^2}$-f model for computing the flow in a 3D wall jet, *In: Fourth International Symposium on Turbulence Heat and Mass Transfer*, (2003).

6. Durbin, P.A. Near-Wall Turbulence Closure Modeling Without "Damping Functions". *Theoretical and Computational Fluid Dynamics*, *3*, pp. 1-13, (1991).
7. Fukasawa, M. and Hayakawa, S. and Saito, M. Thermal-Hydraulic Analysis for Inversely Stratified Molten Corium in Lower Vessel. *Journal of Nuclear Science and Technology*, *45*, pp. 873–888, (2008).
8. Gabor, J.D. and Ellison, P.G. and Cassulo, J.C. Heat transfer from internally heated hemispherical pools, *Proceeding of* 19*th National Heat Transfer Conference*, Orlando, Florida, July 27-30, (1980).
9. Hanjalić,K. One-point closure models for buoyancy-driven turbulent flows. *Annual Reviews of Fluid* Mechanics, *34*, pp. 321–347, (2002).
10. Ince, N and Launder, B. E. On the computation of buoyancy-driven turbulent flows in rectangular enclosures, *International Journal of Heat and Fluid Flow*, *10*, pp. 110–117, (1989).
11. Kenjereš, S. and Hanjalić, K. Prediction of turbulent thermal convection in concentric and eccentric horizontal annuli, *International Journal of Heat and Fluid Flow*, *16*, pp. 429–439, (1995).
12. Kenjereš, S. Numerical modeling of complex buoyancy-driven flows, *Ph.D. Thesis*, Delft University of Technology, Delft, The Netherlands, (1998).
13. Kenjereš, S. and Gunarjo, S.B. and Hanjalić, K. Contribution to elliptic relaxation modeling of turbulent natural and mixed convection, *International Journal of Heat and Fluid Flow*, *26*, pp. 569–586, (2005).
14. Kulacki, F.A. and Goldstein, R.J. Thermal convection in a horizontal fluid layer with uniform volumetric energy sources, *Journal of Fluid Mechanics*, *55* pp. 271–287 (1972).
15. Mayinger, F. and Jahn, M. and Reineke, H.H. and Steinbernner, U. Examination of thermohydraulic processes and heat transfer in a core melt, *BMFT RS*, Hanover FRG, German, (1976).
16. Nourgaliev, R.R. and Dinh, T.N. and Sehgal, B.R. Effect of fluid Prandlt number on heat transfer characteristics in internally heated liquid pools with Rayleigh numbers up to 10^{12}, *Nuclear Engineering and Design*, *169*, pp. 165–184, (1987).
17. Rempe, J. L. and Suh, K. Y. and Cheung, F. B. and Kim, S. B. In-vessel retention of moltetn corium: Lessons learned and outstanding issues, *Nuclear Technology*, *161*, pp. 210–267, (2008).
18. Theofanous, T.G. and Liu, C. and Additon, S. and Angelini, S. and Kymalainen, O. and Salmassai, T. Experience From the First Two Integrated Approaches to In-Vessel Retention Through External Cooling, *OECD/CSNI/NEA Workshop on Large Molten Pool Heat Transfer*, Grenoble, France, March 9-11, (1994).
19. Theofanous, T.G. and Liu, C. Natural convection experiments in a hemisphere with Rayleigh numbers up to 10^{15}, *Proceedings National Heat Transfer Conference*, p. 349, Portland, Oregon, August 5-9, (1995).
20. Thielen, L. and Hanjalić, K. and Jonker, H. and Manceau, R. Predictions of flow and heat transfer in multiple impinging jets with an elliptic-blending second-moment closure, *International Journal of Heat and Mass Transfer*, *48*, pp. 1583–1598, (2005).